Article

Effects of crystallinity of ZSM-5 zeolite on *para*-selective *tert*-butylation of ethylbenzene

PUSHPARAJ Hemalatha [a], MANI Ganesh [a], MUTHIAHPILLAI Palanichamy [a], VELAYUTHAM Murugesan [b], PARK Yong-Ki [c], CHOI Won Choon [c], JANG Hyun Tae [a],*

[a] *Department of Chemical Engineering, Hanseo University, Seosan-si 356 706, South Korea*
[b] *Department of Chemistry, Anna University, Chennai 600 025, India*
[c] *Green Chemistry Research Division, Korea Research Institute of Chemical Technology, Jang-dong 100, Daejeon 305 600, South Korea*

ARTICLE INFO

ABSTRACT

Highly crystalline ZSM-5 zeolites are important for *para*-selective alkylation of alkyl aromatics, because they carry few external acid sites for isomerization of *p*-dialkyl products. Such zeolites (Si/Al = 25, 50, and 75) were synthesized in a fluoride medium between pH 4 and 6. Their crystallinities, crystal sizes, and surface areas were higher than those of a commercial ZSM-5 zeolite. Their *para* selectivities in alkylation were tested for vapor-phase *tert*-butylation of ethylbenzene between 200 and 400 °C. As expected, all the catalysts showed more than 90% *para* selectivity. At 300 °C, ethylbenzene conversion decreased in the order ZSM-5(25, commercial) > ZSM-5(25) > ZSM-5(50) > ZSM-5(75). The catalysts had weak, medium, and strong acid sites, but all the acid sites of ZSM-5(75) were weaker than those of ZSM-5(25) and ZSM-5(50). The high activity of commercial ZSM-5 was caused by its strong acid sites being stronger than those of the synthesized zeolites. Although the activity of the commercial catalyst was higher than those of the present catalysts, the selectivity for 4-*t*-butylethylbenzene (4-*t*-BEB) was low. The optimum feed ratio (ethylbenzene:*t*-butyl alcohol) was 2:1 and the feed rate was 1.65 h⁻¹ for high ethylbenzene conversion and 4-*t*-BEB selectivity. Time-on-stream studies showed slow catalyst deactivation. Highly crystalline ZSM-5 zeolites are therefore better than a commercial zeolite for *para*-selective alkylation of alkyl aromatics. They do not require much post-modification for high *para* selectivity. A fluoride medium is therefore better than an alkaline medium for obtaining highly crystalline *para*-selective ZSM-5 zeolites.

1. Introduction

The alkylation of alkyl aromatics to dialkylated compounds via simple alkylation, *trans* alkylation, or disproportionation is commercially important [1], because of the uses of the dialkyl products; for example, *p*-xylene is used to obtain terephthalic acid, a monomer for terylene [2,3]; *p*-ethyltoluene is used to produce *p*-methylstyrene, the monomer for poly(*p*-methyl-styrene) [4,5]; *p*-diethylbenzene is used to produce divi-nylbenzene, a monomer for cross-linked polystyrene [6]; and other *p*-alkylated ethylbenzenes are used to produce *p*-alkylated styrenes, the monomers for poly(*p*-alkylated sty-renes), which have high glass-transition temperatures (T_g) compared with polystyrene [7]. Zeolites have been widely used

---

as catalysts for alkylation of alkyl aromatics [8]. Dialkylation was reported over X and Y zeolites partly loaded with rare earths [9]. In many alkylation processes, the *meta* isomer, rather than the *ortho* and *para* isomers, is formed, but *para*-selective alkylation has been attempted in most alkylations. *para*-Selective alkylation was first demonstrated by Mobil researchers for the production of *p*-xylene [10,11].

Generally, in an alkylation, alkyl cations attack the 2-, 4-, and 6-positions of alkyl aromatics, as alkyl groups are *ortho*- and *para*-directing. If the alkyl groups are bulky, *para* substitution becomes predominant over *ortho* substitution. However, at high temperatures, 1,4-dialkyl products isomerize to 1,3-dialkyl products on the Brönsted acid sites of zeolites. Since isomerization requires a large amount of space, it is more prevalent in large-pore zeolites. External acid sites also contribute to isomerization and such sites arise as a result of low crystallinity. Hence, for *para*-selective alkylation, a highly crystalline, medium-pore ZSM-5 zeolite is a suitable choice. It can provide selective constrained access to, and egress from, the intra-crystalline free spaces to molecules of size less than the pore size of about 0.55 nm. It is a unique characteristic of ZSM-5 to exhibit *para* selectivity.

For commercial ZSM-5 zeolites, various modification methods have been reported [12–14]. In all of these methods, passivation of the external surface acidity and narrowing of the pore openings [15] were used to enhance the *para* selectivity. However, such modifications drastically reduced conversion. In this context, ZSM-5 zeolites synthesized in fluoride media are convenient substitutes for commercial zeolites. Such zeolites are large crystals, have high crystallinity, and are defect-free, with high surface areas [16–18]. High crystallinity and large crystal size enhance *para* selectivity, and an inverse relationship between the rate of isomerization and crystal radius has been reported in the literature [19–21].

In this study, *tert*-butylation of ethylbenzene was carried out in the vapor phase over ZSM-5 catalysts synthesized in a fluoride medium. 4-*tert*-Butylation of ethylbenzene is important as its dehydrogenated product, 4-*t*-butylvinylbenzene (4-*t*-BVB), is an important monomer for the commercial production of poly(4-*t*-butylstyrene), which has a high T_g value. The same reaction was also studied over Al-MCM-41, and high *para* selectivity was reported [22]. Bidart et al. [23] studied *tert*-butylation of ethylbenzene over FeY zeolite and reported mainly monoalkylation. There have been no reports of the same reaction over ZSM-5 synthesized in a fluoride medium.

A major stumbling block in the synthesis of ZSM-5 in a fluoride medium is the reduced amount of aluminum transport from the gel to the framework as a result of the formation of AlF_x species. In our laboratory, this problem was solved by using phosphate as a co-complexant to fluoride. Syntheses of ZSM-5 were also carried out using different silicon sources to select the best source for high crystallinity.

2. Experimental

2.1. Materials

Tetraethyl orthosilicate (TEOS; 98%), tetrapropylammonium bromide (98%), aluminum sulfate octadecahydrate (98%), ammonia (28%), ammonium fluoride (99%), and sodium aluminate (50–56% Al_2O_3) (all obtained from Aldrich), as well as orthophosphoric acid (85%) and hydrofluoric acid (48%) (both obtained from Merck), were used in the syntheses. LUDOX-ammonium-stabilized colloidal silica (AS silica; 40 wt% suspension in water), LUDOX-sodium-stabilized colloidal silica (HS silica; 40 wt% suspension in water), fumed silica, and sodium silicate (~26.5% SiO_2) (all obtained from Aldrich) were used as silicon sources in the syntheses. Potassium hydroxide (90%; Aldrich) was used in potentiometric titrations. The chemicals used in the catalytic reactions, i.e., ethylbenzene and *t*-butyl alcohol, were of Merck grade.

2.2. Optimization of fluoride content for ZSM-5 syntheses

The following gel composition was used [16] for the ZSM-5 syntheses in a fluoride medium: 0.07 $C_{12}H_{28}NBr$:1.0 SiO_2:0.006 Al_2O_3:x NH_4F:80 H_2O.

The syntheses were carried out initially with TEOS and sodium aluminate as the sources for silicon and aluminum, respectively. Tetrapropylammonium bromide was used as a structure-directing template. To optimize the fluoride content for the syntheses, the F/Si ratio was altered using NH_4F; the weights are given in Table 1.

In a typical synthesis, sodium aluminate (0.022 g), an appropriate amount of ammonium fluoride, tetrapropylammonium bromide (0.462 g), and water (35 g) were mixed in a 100 ml beaker and stirred for 5 h. TEOS (5.16 g) was added drop-wise. Stirring was continued for 3 h. Finally, the pH of the mixture was reduced to 7.0 by adding two or three drops of hydrofluoric acid, and stirring was continued for 1 h. The resulting gel was autoclaved and hydrothermal crystallization was carried out at 170 °C for 5 d in a static oven. The crystallized product was recovered by filtration, washed repeatedly with water, dried at 110 °C in the oven for 12 h, and calcined at 650 °C in air for 8 h.

2.3. Syntheses of ZSM-5 in fluoride medium with phosphate

Sodium aluminate was replaced by aluminum sulfate. Phosphate was used as well as fluoride. Tetrapropylammonium bromide was used as a structure-directing agent and the gel composition was as follows: 0.07 $C_{12}H_{28}NBr$:1 SiO_2:0.02 Al_2O_3:1.3 NH_4F:0.02 P_2O_5:80 H_2O.

In a typical synthesis, aluminum sulfate (0.330 g), orthophosphoric acid (0.056 g), tetrapropylammonium bromide

Table 1
Weights of NH_4F used in ZSM-5 syntheses.

F/Si ratio	Weight of NH_4F (g)
0.3	0.27
0.6	0.54
1.0	0.90
1.3	1.17
1.6	1.44
2.0	1.80

(0.462 g), and water were mixed in a 100 ml beaker and stirred. Ammonium fluoride (1.17 g) was then added to the mixture. TEOS (5.16 g) was added and stirring was continued for 3 h. The resulting gel was transferred to a Teflon-lined stainless-steel autoclave and hydrothermal crystallization was carried out at 170 °C for 5 d in a static oven. The crystallized product was recovered by filtration, dried at 110 °C for 12 h, and calcined at 650 °C in air for 8 h. The same procedure was repeated with appropriate quantities of aluminum sulfate to obtain ZSM-5 with Si/Al = 50 and 75.

2.4. Syntheses of ZSM-5 in fluoride medium with different silicon sources

Syntheses of ZSM-5 in a fluoride medium were performed using different sources of silicon (TEOS, sodium silicate, AS silica, HS silica, and fumed silica). The following gel composition was used: 0.07 $C_{12}H_{28}NBr$:1.0 SiO_2:0.02 Al_2O_3:1.3 NH_4F:0.02 P_2O_5:80 H_2O.

In a typical procedure, aluminum sulfate (0.330 g), orthophosphoric acid (0.056 g), tetrapropylammonium bromide (0.462 g), and water (35 g) were mixed in a 100 ml beaker and stirred for 2 h. Ammonia (1:1) was added to give a faint permanent precipitate. After 30 min of stirring, ammonium fluoride (1.17 g) was added. After 5 h of stirring, an appropriate amount of silica source was added and stirring was continued for another 5 h. The resulting gel was transferred to a Teflon-lined stainless-steel autoclave, and hydrothermal crystallization was carried out at 170 °C for 5 d in a static oven. The crystallized product was recovered by filtration, dried in an oven at 110 °C for 12 h, and calcined at 650 °C in air for 8 h.

2.5. Potentiometric titrations

To establish complexation between phosphate and Al^{3+} during the ZSM-5 synthesis, potentiometric titrations were carried out. Potentiometric titrations of orthophosphoric acid (0.02 mol/L) versus potassium hydroxide (0.6 mol/L), and orthophosphoric acid plus Al^{3+} (0.0475 mol/L) versus potassium hydroxide, were carried out using a pH meter (Toshniwal) provided with a combined glass electrode. The titrations were carried out in a double-walled 100 ml beaker provided with an inlet and an outlet for water circulation. The temperature was maintained at 30 °C, with an ionic strength of 0.5 mol/L. The equilibrium pH was measured for each addition of potassium hydroxide. The measured pH was plotted against the volume of alkali added to establish complex formation between phosphate and Al^{3+}.

2.6. Catalyst characterization

The synthesized products were identified and their crystallinities were determined by powder X-ray diffraction (XRD) analysis. The XRD patterns were acquired on a PANalytical X'pert PRO diffractometer equipped with a Cu K_α (0.154 nm) radiation source and a liquid-cooled germanium solid-state detector. The samples were scanned from 5° to 40° (2θ) in

steps of 0.002 nm, with a count time of 5 s at each point. For the crystallinity calculations, the intensities of the peaks from (−101), (011), (051), and (−501) were compared with those from a commercial catalyst. The specific surface areas of the samples were measured by nitrogen adsorption at −196 °C using a Belsorp Mini II sorption analyzer. Prior to measurements, the samples were heated for 4 h in vacuum at 400 ºC. The surface areas were determined by the Brunauer-Emmett-Teller (BET) method. The morphologies and size changes of the prepared zeolite samples were studied using scanning electron microscopy (SEM; JEOL JSM 5600). The Si/Al ratios of the samples were determined using an energy-dispersive X-ray (EDS) analyzer in the SEM chamber.

Temperature-programmed desorption of ammonia (NH_3-TPD) was performed using a BELCAT-M catalyst analyzer equipped with a thermal conductivity detector. The catalyst sample (0.2 g) was placed in the microreactor and treated at 430 °C for 3 h under a He flow, followed by sorption of dry ammonia at 100 °C in a static system for 90 min and 1.5 bar ammonia pressure. Stripping was then performed for 40 min at 100 °C under a He flow. In this way, weakly physically adsorbed ammonia in the sample was avoided. Desorption of ammonia was carried out at a rate of 10 °C/min from 100 °C up to 650 °C under an He flow (50 ml/min).

Solid-state nuclear magnetic resonance (NMR) spectra of ZSM-5 were obtained under magic-angle spinning (MAS) conditions, at ambient temperature, on a Bruker MSL 500 spectrometer. The ^{27}Al MAS-NMR spectra were recorded at a resonance frequency of 130.32 MHz, with short 2.1 μs pulse and a recycle delay of 0.1 s. The typical rotational frequency was ca. 10 kHz, using a zirconia rotor of diameter 4 mm, and 12500 scans were necessary to obtain a well-resolved spectrum. ^{27}Al chemical shifts were reported in relation to a liquid solution of aluminum nitrate. ^{29}Si MAS-NMR spectra were recorded at a resonance frequency of 99.361 MHz on a Bruker MSL 500 spectrometer, with a short pulse of 4 μs, a recycle delay of 30 s, and 2500 scans. The typical rotational frequency was about 4.5 kHz, using a zirconia rotor of diameter 7 mm. Chemical shifts were given in ppm from standard tetramethylsilane.

2.7. Catalytic activity measurements

Tert-butylation of ethylbenzene with *t*-butyl alcohol as the alkylating agent was carried out on a fixed-bed vertical down-flow reactor of internal diameter 2 cm. About 0.5 g of the catalyst was placed in the reactor and supported on either side by a thin layer of quartz wool and ceramic beads. The reactor was heated to the requisite temperature using a temperature-programmed furnace. The catalyst was activated at 500 °C for 6 h in a controlled stream of air. The reactants were fed into the reactor using a syringe infusion pump. The products collected in the receiver flask were analyzed in a Shimadzu 17-A gas chromatograph equipped with a DB column and a flame ionization detector. The products were also identified using gas chromatography-mass spectrometry (Perkin Elmer Clarus 500).
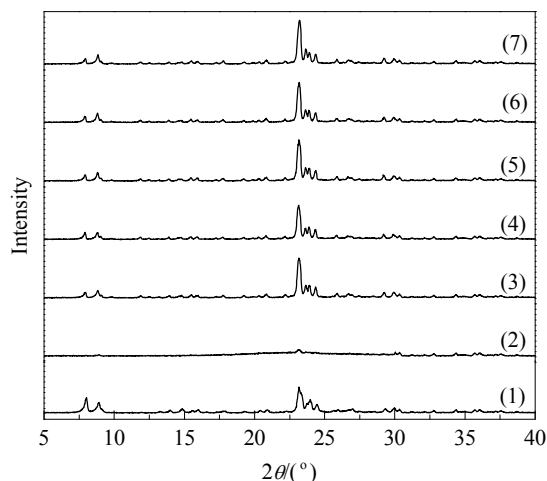
Fig. 1. XRD patterns of commercial ZSM-5(25) (1) and ZSM-5 synthesized with F/Si ratios of 0.3 (2), 0.6 (3), 1.0 (4), 1.3 (5), 1.6 (6), and 2.0 (7).
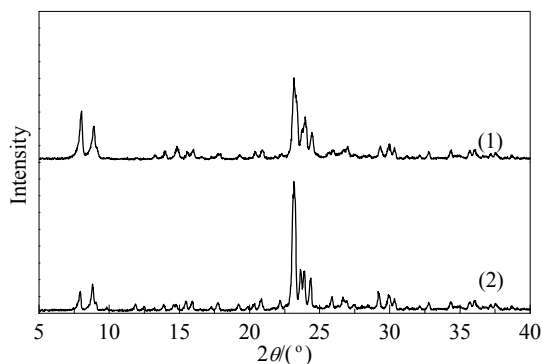

Fig. 3. XRD patterns of commercial ZSM-5(25) (1) and ZSM-5 synthesized with TEOS (2), HS silica (3), sodium silicate (4), AS silica (5), and fumed silica (6) as silicon sources.

3. Results and discussion
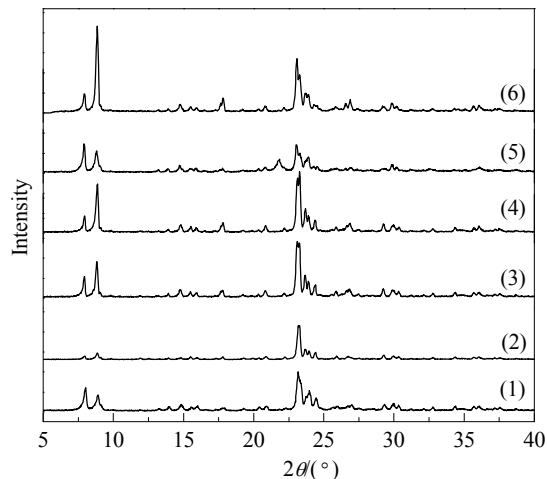
3.1. Catalyst characterization results

3.1.1. XRD

The powder XRD patterns of ZSM-5 zeolites, synthesized in a fluoride medium with different fluoride contents, are presented in Fig. 1. The XRD pattern of commercial ZSM-5 is also presented in the same figure for comparison. The reflections in the XRD patterns of the synthesized samples were higher than those of the commercial sample. The fluoride medium was therefore proved to enhance the crystallinity of ZSM-5 [24,25]. The interactions of fluoride with both silicon and aluminum, facilitating their slow release for zeolite construction, are suggested as the main cause of the high crystallinity. Based on the intensity of the patterns, the optimum F/Si ratio for crystallization was in the range 1.0 to 1.6. A similar range was also reported by Louis and Kiwi-Minsker [24].

In fluoride-mediated synthesis, the acidity has been reported to be low as a result of formation of AlF_x species [25]. To suppress formation of such AlF_x species, a co-complexant to fluoride, namely phosphate, was used during the synthesis of

Fig. 2. XRD patterns of commercial ZSM-5(25) (1) and synthesized ZSM-5(25) (2).

ZSM-5(25). Its XRD pattern, shown in Fig. 2(2), displayed high crystallinity for all reflections.

The XRD patterns of ZSM-5 zeolites synthesized with different silicon sources are shown in Fig. 3. All the patterns showed the peaks characteristic of ZSM-5 reported in the literature [26,27]. The pattern derived from TEOS yielded more intense reflections than those from other silicon sources, therefore it was chosen for the bulk synthesis of ZSM-5 (Si/Al = 25, 50, and 75). Ethanol, released from the hydrolysis of TEOS, reduced the dielectric constant of the medium, and enhanced the formation of highly crystalline zeolites. Sano et al. [28] reported the synthesis of large mordenite crystals in the presence of aliphatic alcohols. Slow dissolution of a gel and release of silicon and aluminum species enhanced the crystal size. The intensities of the peaks from (051) in Fig. 3(2), (3), and (4) were higher than those in Fig. 3(5) and (6). A low dielectric constant or sodium content in the medium was therefore suggested to play a characteristic role in enhancing crystallinity during synthesis. In addition, it was also seen to aid enhanced growth of (011). Therefore the sodium content, as well as the alcohol content, enhanced growth along the (051) and (011) directions compared with the other directions. Figure 3(6) shows more intense reflections than Fig. 3(5). The ammonium content of the synthesis gel with fumed silica was lower than that of the gel with AS silica, hence ammonium was also important in enhancing intensity. The synthesis gel with AS silica, which has a higher ammonium content than fumed silica, yielded low crystallinity ZSM-5 crystals, but a high ammonium content was seen to aid growth of (−101) compared with (011). So, from this analysis, it was verified that a synthesis gel with a low dielectric constant, and a high sodium content or low ammonium content, yielded highly crystalline ZSM-5 zeolites.

The XRD patterns of the ZSM-5(25), (50), and (75) synthesized in a fluoride medium are presented in Fig. 4. The pattern of commercial ZSM-5 is also shown for comparison. Based on the intensities of the dominant XRD peaks, the crystallinities of all the ZSM-5 samples were calculated, and the values are pre-
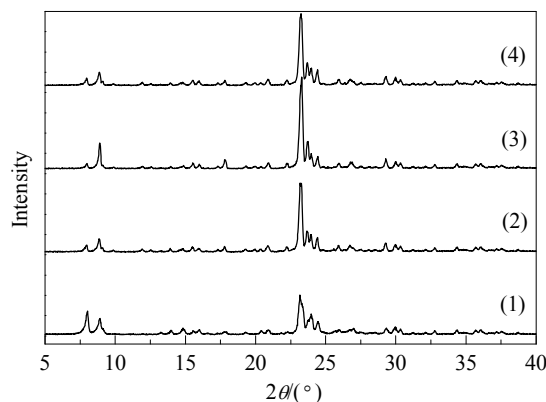
Fig. 4. XRD patterns of commercial ZSM-5(25) (1) and synthesized ZSM-5(25) (2), ZSM-5(50) (3), and ZSM-5(75) (4).

Fig. 5. N$_2$ adsorption-desorption isotherms of the synthesized zeolites.

sented in Table 2. For the calculations, the crystallinity of the commercial ZSM-5 was taken as 100%. As expected, the synthesized samples showed higher crystallinities than the commercial ZSM-5. This was also verified by SEM analysis, as discussed below.

3.1.2. BET analysis

The N$_2$ adsorption-desorption isotherms of the synthesized zeolites are shown in Fig. 5. All the isotherms showed type I adsorption. The adsorption isotherms matched the desorption isotherms in all three cases. The knee portion of the ZSM-5(75) isotherm was lower than those of ZSM-5(25) and ZSM-5(50), indicating its lower surface area, as shown in Table 2. The isotherms also showed a lower micropore volume for ZSM-5(75) than for the others. The isotherms also showed a slightly higher surface area and pore volume for ZSM-5(50) than for ZSM-5(25) and ZSM-5(75).

3.1.3. Potentiometric investigation of phosphate complexation of aluminum

The pH-volume curves for the titration of orthophosphoric acid versus potassium hydroxide, and orthophosphoric acid plus Al^{3+} versus potassium hydroxide, are shown in Fig. 6. In the titration of orthophosphoric acid, three buffer regions were identified, and the pK_a values of 2.12 (pK_a1), 7.21 (pK_a2), and 12.30 (pK_a3) derived from them were comparable to those reported in the literature [29]. The titration curve of orthophosphoric acid plus Al^{3+} versus potassium hydroxide followed nearly the same trend as that of orthophosphoric acid versus potassium hydroxide, except that a fourth buffer region occurred at around pH 9.7, and there was a slight shift of the curve to lower pH. This established the formation of a phosphate-aluminum complex.
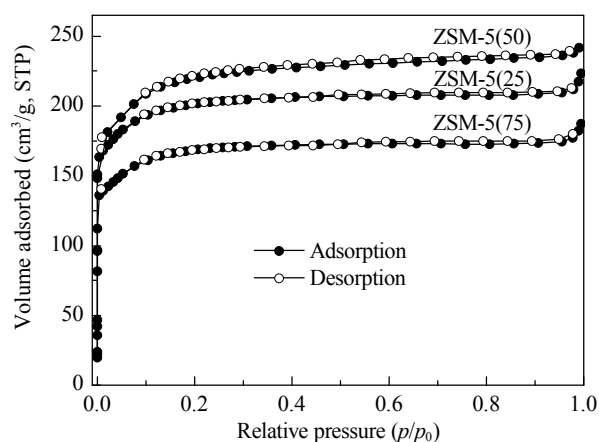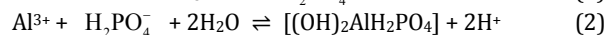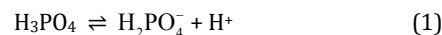
As shown in Eqs. (1) and (2), complex formation between Al^{3+} and phosphate and hydrolysis of aluminum phosphate (Eq. 2) in the pH region between 2.20 and 3.35 released a larger number of protons than free orthophosphoric acid, and reduced the pH.

$$H_3PO_4 \rightleftharpoons H_2PO_4^- + H^+ \qquad (1)$$
$$Al^{3+} + H_2PO_4^- + 2H_2O \rightleftharpoons [(OH)_2AlH_2PO_4] + 2H^+ \qquad (2)$$

When the pH was increased to 6.73–7.5, a second dissociation occurred (the second buffer region), according to Eqs. (3) and (4). If the complex [(OH)$_2$AlH$_2$PO$_4$] has the same acidity as H$_2$PO$_4^-$, then the buffer region in the curve of orthophosphoric acid and that of orthophosphoric acid plus Al^{3+} coincide. However, a decrease in pH was observed for the latter compared with the former. The dissociation constant of [(OH)$_2$AlH$_2$PO$_4$] may therefore be higher than that of H$_2$PO$_4^-$. Delocalization of the oxygen lone pair of the Al–O–P linkage in the aluminum vacant 3p orbital resulted in a higher dissociation constant than that of H$_2$PO$_4^-$.

$$H_2PO_4^- \rightleftharpoons HPO_4^{2-} + H^+ \qquad (3)$$
$$[(OH)_2AlH_2PO_4] \rightleftharpoons [(OH)_2AlHPO_4]^- + H^+ \qquad (4)$$
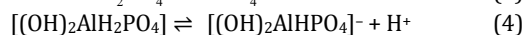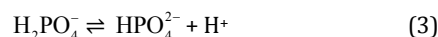
When the pH was increased to 9.60–10.19, a third dissociation occurred (third buffer region), according to Eq. (5). This

Table 2
Percentage crystallinities and BET results for ZSM-5 zeolites.

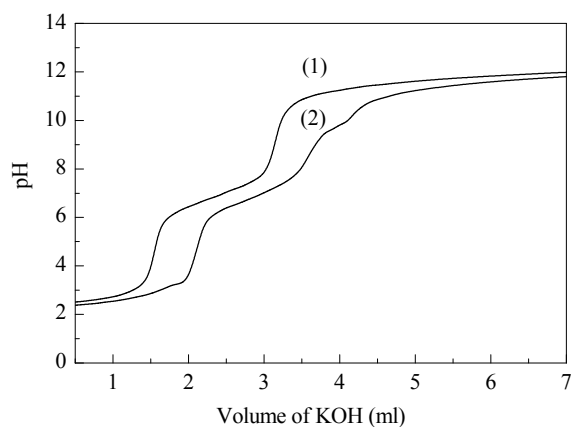| Catalyst	Crystallinity (%)	Surface area (m^2/g)	Pore volume (cm^3/g)
ZSM-5(25) (Commercial)	100	430	0.163
ZSM-5(25)	117	750	0.259
ZSM-5(50)	124	790	0.280
ZSM-5(75)	120	634	0.214

Fig. 6. Plot of pH versus volume of alkali for orthophosphoric acid versus potassium hydroxide (1) and orthophosphoric acid plus Al^{3+} versus potassium hydroxide (2).
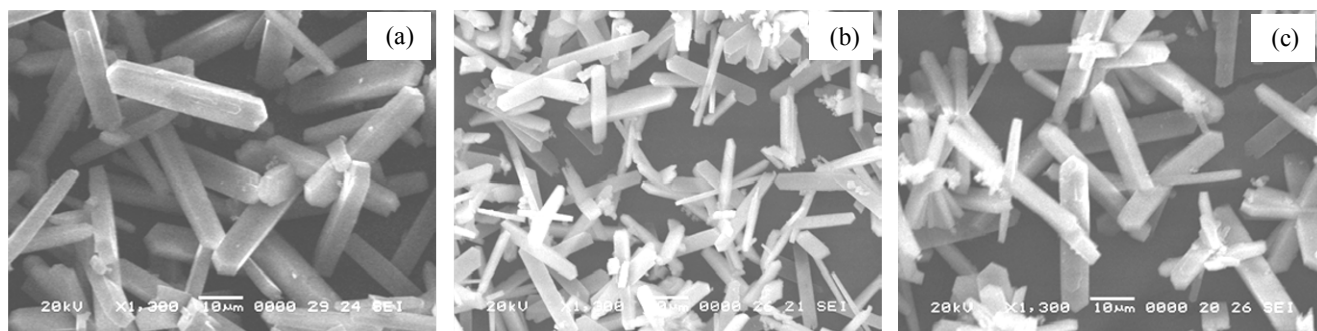
Fig. 7. SEM images of the synthesized ZSM-5(25) (a), ZSM-5(50) (b), and ZSM-5(75) (c).

buffer region did not exist in the titration of orthophosphoric acid itself, and was observed only in the titration of orthophosphoric acid plus Al^{3+}. The dissociation of $[(OH)_2AlHPO_4]^-$ species was confirmed by the formation of a clear solution. This was noted in the titration of Al^{3+} plus orthophosphoric acid, but not in the titration of orthophosphoric acid itself.

$$[(OH)_2AlHPO_4]^- \rightleftharpoons [O^-(OH)AlHPO_4]^{2-} + H^+ \qquad (5)$$
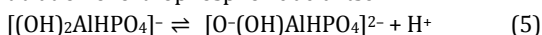
If the pH was further increased to 11.30–12.22, a fourth dissociation occurred (fourth buffer region), as shown in Eq. (6). Here again, the buffer region for the titration of Al^{3+} plus orthophosphoric acid occurred at a lower pH than that of orthophosphoric acid. This again established complexation between Al^{3+} and phosphate.

$$[O^-(OH)AlHPO_4]^{2-} \rightleftharpoons [O^-(OH)AlPO_4]^{3-} + H^+ \qquad (6)$$
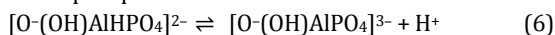
These results established the formation of a stable phosphate complex with Al^{3+}. Formation of such a complex is the reason for transportation of aluminum from the gel to the framework.
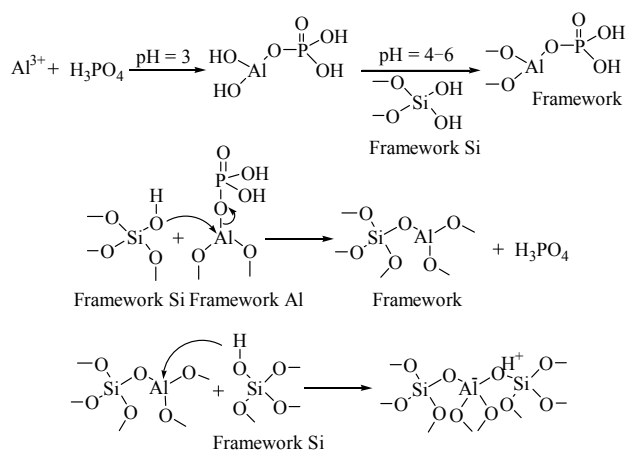
3.1.4. SEM and EDS analyses

The SEM images of ZSM-5(25), (50), and (75) are shown in Fig. 7. They show elongated prismatic crystals. The crystals of ZSM-5(75) were slightly smaller than those of the others. This verified that the Si/Al ratio in the gel influences the crystal dimensions. As a gel with a high silica content takes longer to mineralize with fluoride, the crystallization time would also be longer than those for gels with low silica contents. This resulted in smaller crystal sizes for ZSM-5(75) than for the others. The crystal terraces in all the images were smooth, without any deposits. The tiny crystallites of ZSM-5(75) were the result of incomplete crystallization. Similar images were also obtained by Arichi and Louis [30].

To compare the Si/Al ratios of the synthesized zeolites with those of their mother liquids, EDS analyses were carried out. The results are given in Table 3. The Si/Al ratios of the synthe-

sized zeolites were slightly lower than those of the mother liquids. Complete transportation of aluminum from the mother liquid to the framework and a slightly reduced amount of silicon in the framework were therefore observed. In contrast to the previous report of formation of AlF_x, which reduced the framework Al^{3+} content [25], the use of phosphate increased the content. These results therefore clearly established the influence of phosphate on the AlF_x equilibria and on the transportation of aluminum from the gel to the framework. The results also showed the absence of phosphate in the zeolite framework, even though the potentiometric titrations established bonding between aluminum and phosphate across the entire pH range. Phosphate remains in the coordination sphere of aluminum even if the latter is bonded to two silicate units, as shown in Scheme 1. When aluminum acquires a fourth coordination in the zeolite framework, phosphate will be immediately expelled, leaving aluminum in the trigonal planar state again. Tetrahedral coordination is therefore only allowed by chelating silicate units, and not by monodentate ligands such as phosphate.

3.1.5. NH₃-TPD

The NH_3-TPD results are shown in Fig. 8. In the evaluation of zeolite acidity by NH_3-TPD, three types of acid sites were suggested, based on the temperature range of ammonia desorption: weak acid sites, when the desorption occurs between 150 and 250 °C, medium acid sites for desorption between 250 and 350 °C, and strong acid sites for desorption between 350 and

Table 3
Results of EDS analyses.

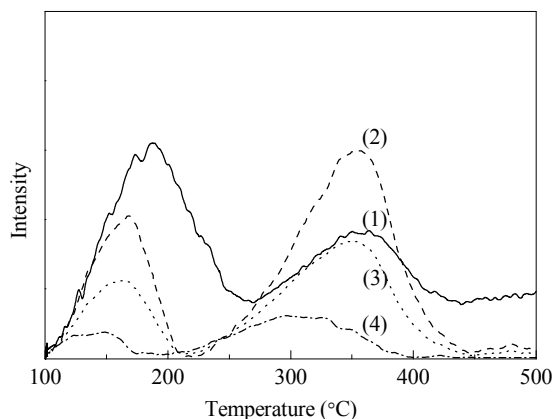| Catalyst	Si/Al ratio		Atomic content by EDS (%)			
	Mother liquid	By EDS	Si	Al	O	P
ZSM-5(25) (Commercial)	25	—	—	—	—	—
ZSM-5(25)	25	22.0	14.7	0.7	84.6	0.0
ZSM-5(50)	50	38.0	21.0	0.6	78.5	0.0
ZSM-5(75)	75	52.7	20.0	0.4	79.5	0.0

Scheme 1. Phosphate complexation of aluminum.

Fig. 8. NH₃-TPD profiles of commercial ZSM-5(25) (1) and the synthesized ZSM-5(25) (2), ZSM-5(50) (3), and ZSM-5(75) (4).

450 °C [31–33]. The peak between 100 and 210 °C for the weak acid sites was clearly resolved for the synthesized zeolites, but those of the medium and strong acid sites between 210 and 450 °C overlapped significantly. The quantity of weak acid sites was lower than those of medium and strong acid sites. An additional role of the fluoride medium is therefore to create larger numbers of acid sites in the channel intersections, the regions for strong acid sites, than along the channels, the regions for weak acid sites. It has also been reported that in zeolites, 75% of total acid sites were present in channel intersections and the rest along the channels [34]. This was verified for the synthesized zeolites in this study, because there were more medium and strong acid sites than weak acid sites. The NH₃-TPD profiles also illustrated that with increasing Si/Al ratio, the quantity of strong acid sites, corresponding to desorption between 350 and 450 °C, decreased. In addition, the desorption shifted from 450 to 400 °C with increasing Si/Al ratio, and this was clearly seen for ZSM-5(75). It is difficult to understand why this was not also observed for ZSM-5(25) and (50), for which only the densities were affected, not the strengths. The Si/Al ratio alone is therefore not the controlling factor for the strengths of the acid sites; the densities of acid sites located in the channel intersections are also important. If the Si/Al ratio of the zeolite is above 50, the acid sites are weak/medium, irrespective of their location, therefore the higher the Si/Al ratio (particularly above 50), the fewer the number of acid sites, even in the channel intersections, and the greater the decrease in the strengths of such sites. Such a decrease was also noted for the weak acid sites; again, this was clearly observed for ZSM-5(75). So, with increasing Si/Al ratio, the acid sites are located far off, and they are weaker than those of zeolites with lower Si/Al ratios. Again, the weak acid sites of ZSM-5(25) and (50) showed only a decrease in the density, not in the strength, unlike the medium and strong acid sites. Diffuse reflectance infrared Fourier transform (DRIFT) is a technique used to study acidity, using pyridine and other bulky amines. Bulky amines are important in determining the external surface acidity, which confirm the crystallinity, but DRIFT facilities were not available.

The results for the commercial ZSM-5(25) zeolite are also shown in Fig. 8. The intensities of the peaks from the medium and strong acid sites were lower than those for the synthesized ZSM-5(25). Here, too, the peaks from the medium and strong acid sites overlapped, but desorption of ammonia extended above 400 °C. The strong acid sites of the commercial catalyst might therefore be stronger than those of the synthesized ZSM-5(25) and (50) catalysts. This indicates a high density of acid sites in the channel intersections in the commercial catalyst. The absence of desorption was the result of adsorption-desorption equilibrium of ammonia. The desorption peak from the weak acid sites was more intense than those of the synthesized zeolites. The desorption also extended above 200 °C, hence these acid sites were more acidic than those of the synthesized zeolites. As the weak acid sites are located along the channels, the density might be high enough to increase their strength. So, it was expected that the commercial zeolite might be more active than the synthesized zeolites in the *tert*-butylation of ethylbenzene.

3.1.6. ²⁷Al MAS-NMR and ²⁹Si MAS-NMR

The ²⁷Al MAS-NMR and ²⁹Si MAS-NMR spectra of ZSM-5(25) is shown in Fig. 9. In Fig. 9(a), the intense sharp peak centered at $\delta = 52$ arose from the tetrahedrally coordinated framework aluminum [35]. As there was no peak close to $\delta = 0$, non-framework alumina was proved to be absent. Dislodging of aluminum from the framework during calcination was therefore ruled out. The result also confirmed the thermal stability of ZSM-5 synthesized in a fluoride medium.

The peak at $\delta = -106$ in Fig. 9(b) was from Q³ species [Si–(OSi)₃(OAl)] and that at $\delta = -112$ was from Q⁴ species [Si(OSi)₄] [17,36]. As there was no peak below $\delta = -106$ (close to $\delta = -103$), there were not significant numbers of defective Si–OH groups. This is important evidence of high crystallinity of the zeolite, as discussed above.

3.2. Catalytic studies

Vapor-phase *tert*-butylation of ethylbenzene with *t*-butyl alcohol was studied over commercial ZSM-5(25) and the synthesized ZSM-5(25), ZSM-5(50), and ZSM-5(75) between 200 and 400 °C. The reaction parameters were optimized for maximum ethylbenzene conversion and high selectivity for 4-*t*-BEB. The effects of temperature, feed ratio, weight hourly space ve-
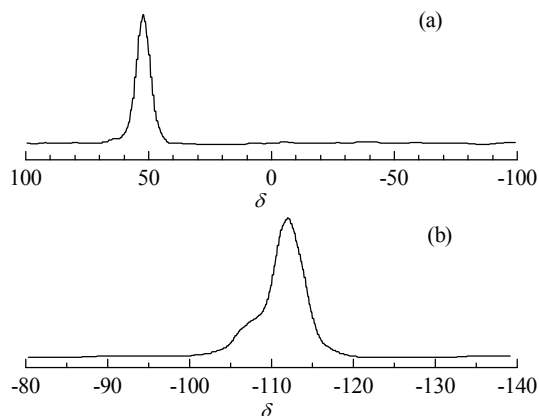

Fig. 9. ²⁷Al MAS-NMR (a) and ²⁹Si MAS-NMR (b) spectra of ZSM-5(25).

Table 4
Effects of temperature on ethylbenzene conversion and product selectivity.

Catalyst	Temperature (°C)	Ethylbenzene conversion (%)	Selectivity (%)						
			1,2-DEB	1,3-DEB	1,4-DEB	3-*t*-BEB	4-*t*-BEB	4-*t*-BVB	Benzene
ZSM-5(25)	200	39.1	4.3	2.2	6.8	10.0	74.1	—	2.6
(Commercial)	250	44.3	3.0	1.1	8.3	19.8	64.0	—	3.8
	300	55.9	1.6	2.6	11.9	17.2	61.3	—	5.4
	350	49.4	1.5	3.9	12.0	18.8	22.2	29.5	12.1
	400	32.2	1.4	6.0	11.7	22.9	5.2	27.9	24.9
ZSM-5(25)	200	33.5	—	—	—	5.1	94.9	—	—
	250	41.7	—	—	—	6.7	93.3	—	—
	300	49.3	—	—	—	7.6	92.4	—	—
	350	44.1	—	—	—	9.0	91.0	—	—
	400	28.0	—	—	—	11.3	88.7	—	—
ZSM-5(50)	200	30.3	—	—	—	7.2	92.8	—	—
	250	38.2	—	—	—	8.3	91.7	—	—
	300	41.6	—	—	—	10.1	89.9	—	—
	350	39.9	—	—	—	13.2	86.8	—	—
	400	30.4	1.3	4.2	2.0	14.9	73.6	—	4.0
ZSM-5(75)	200	25.3	—	—	—	8.3	91.7	—	—
	250	31.7	—	—	—	10.4	89.6	—	—
	300	38.3	—	—	—	12.3	87.7	—	—
	350	36.5	2.2	5.1	4.2	14.5	69.5	—	4.5
	400	33.8	3.2	6.9	5.1	17.8	59.7	—	7.3

Reaction conditions: feed ratio ethylbenzene:*tert*-butyl alcohol = 1:1; WHSV = 1.65 h⁻¹.

locity (WHSV), and time-on-stream on conversion and product selectivity were examined; the results are discussed below.

3.2.1. Effects of temperature

tert-Butylation of ethylbenzene with *t*-butyl alcohol was carried out over commercial ZSM-5(25) at 200, 250, 300, 350, and 400 °C. The products were 1,2-diethylbenzene (DEB), 1,3-DEB, 1,4-DEB, 3-*t*-BEB, 4-*t*-BEB, 4-*t*-BVB, and benzene. The conversions of ethylbenzene and the selectivities for different products are presented in Table 4. The conversion increased from 200 to 300 °C, but decreased at 350 and 400 °C as a result of blocking of active sites by polybutene [37] and/or coke. Coke was also observed between 200 and 300 °C, but to a lesser extent than between 350 and 400 °C. A plausible pathway for *tert*-butylation of ethylbenzene is shown in Scheme 2. *t*-Butyl alcohol is chemisorbed on the Brönsted acid site of zeolites to form *t*-butyl cations. The electrophilic reaction between ethylbenzene and *t*-butyl cations yields 4-*t*-BEB.

In addition to *tert*-butylation of ethylbenzene, disproportionation of ethylbenzene was also observed, but was minimal. The disproportionation of ethylbenzene can occur as shown in Scheme 3. Ethylbenzene is chemisorbed on the Brönsted acid sites of ZSM-5 to form benzene and ethyl cations. Electrophilic reaction between ethyl cations and ethylbenzene yields diethylbenzene isomers, i.e., 1,2-DEB, 1,3-DEB, and 1,4-DEB. The ethyl cations formed by de-ethylation of ethylbenzene attack at the *ortho*- and *para*-positions of ethylbenzene to form 1,2-DEB and 1,4-DEB, respectively. As the *meta*-position of ethylbenzene is not favored for electrophilic attack, 1,3-DEB has to be formed by isomerization of 1,4-DEB or 1,2-DEB on the external surface of the zeolite.

Since the kinetic diameter of 1,2-DEB is 0.68 nm, it can be formed in the channel intersections, but it cannot diffuse out of the crystals. 1,4-DEB can be formed either in the channel intersections or along the channels, and it can freely diffuse out, as its kinetic diameter is 0.58 nm. 1,3-DEB, with a kinetic diameter of 0.68 nm, can be formed by isomerization of 1,4-DEB or 1,2-DEB on the external surfaces or in the channel intersections. The selectivity for 1,2-DEB was very low, as it was formed on the external surfaces, and some of it isomerized to 1,3-DEB. The slight decrease in selectivity for 1,2-DEB from 200 to 400 °C was the result of increased steric hindrance for substitution at the *ortho* position as a result of free rotation of the ethyl group about the C–C bond. Such free rotation of alkyl groups in alkyl aromatics has been reported previously [38]. At low temperatures, the rotation would be slow, but at high temperatures it would be rapid, thus significantly suppressing substitution at both *ortho* positions. The formation of free benzene also supported disproportionation of ethylbenzene. The
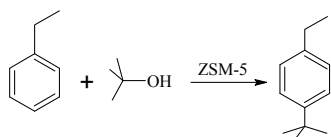
Scheme 2. Formation of 4-*t*-BEB.
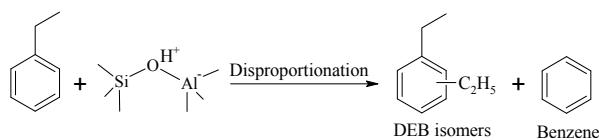
Scheme 3. Disproportionation of ethylbenzene.
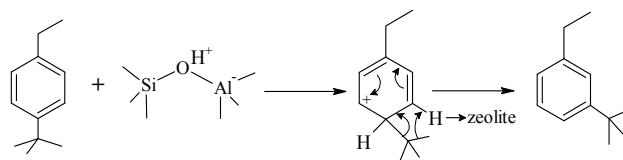
Scheme 4. Isomerization of 4-*t*-BEB to 3-*t*-BEB.
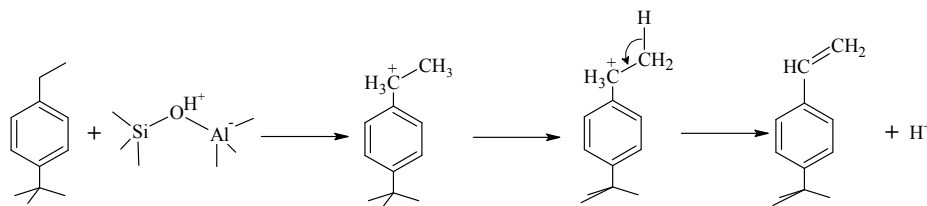
Scheme 5. Carbenium/carbonium ion mechanism.

selectivity for 4-*t*-BEB decreased with increasing temperature as a result of isomerization to form 3-*t*-BEB.

The isomerization of 4-*t*-BEB proceeds as shown in Scheme 4. 4-*t*-BEB is chemisorbed on the Brönsted acid sites of ZSM-5. Protonation of 4-*t*-BEB occurs on the carbon that carries the *t*-butyl group. Reorganization of bonds results in the migration of the *t*-butyl group to the *meta* position to form 3-*t*-BEB. Such a mechanism has already been reported [22]. The *meta* isomers are thermodynamically more stable than the *para* isomers, and this becomes the driving force for isomerization, so the selectivity for 3-*t*-BEB increases with increasing temperature. The molecular size of 3-*t*-BEB (0.68 nm) is higher than the zeolite pore size. Isomerization of 4-*t*-BEB to 3-*t*-BEB can therefore only occur on the external surface of the zeolite. An unexpected product is 4-*t*-BVB, so there is dehydrogenation of the ethyl group of 4-*t*-BEB to 4-*t*-BVB. Such dehydrogenation has been reported to result from the presence of non-framework alumina in mesoporous AlMCM-41 [22], so the catalyst might have non-framework alumina. In the absence of it, dehydrogenation is suggested to occur by a carbenium/carbonium ion mechanism (Scheme 5). A proton is transferred to the methylene group of 4-*t*-BEB to form a pentacoordinated transition state. This decomposes to form a carbenium ion, which subsequently releases an α-hydrogen to form 4-*t*-BVB. However, such dehydrogenation was not observed for ethylbenzene, as styrene was not observed. Hence, the *para* *t*-butyl group of 4-*t*-BEB might activate formation of 4-*t*-BVB. Since the *t*-butyl group is inductively electron-repelling, it enhances the electronic cloud on the methylene group and facilitates proton transfer to the methylene from the zeolite.

The same reaction was also studied over synthesized ZSM-5(25), ZSM-5(50), and ZSM-5(75). The results are also presented in Table 4. These catalysts showed variations in the conversions of ethylbenzene similar to those of the commercial catalyst. The conversion increased from 200 to 300 °C and decreased thereafter. ZSM-5(25) showed a higher conversion than others as a result of a higher density of acid sites. Although the acidity of ZSM-5(50) was 50% less than that of ZSM-5(25), the conversion at 300 °C was not 50% lower. This is because of slow diffusion of reactants along the channels in ZSM-5(50) as a result of its higher hydrophobicity. An important observation in the reactions over ZSM-5 catalysts synthesized in a fluoride medium was the complete absence of dehydrogenation and disproportionation at 300 °C. Disproportionation of ethylbenzene can occur either inside or outside the pores, but acid sites must be available. Since *t*-butyl alcohol is better chemisorbed than ethylbenzene on Brönsted acid sites, disproportionation of ethylbenzene is avoided over all the catalysts. The selectivity

for 3-*t*-BEB increased with increasing temperature over all the catalysts. ZSM-5(75) showed a slightly higher selectivity for 3-*t*-BEB than the others, but a lower selectivity than commercial ZSM-5. Since it is more hydrophobic than the others, it can better retain 4-*t*-BEB and promote isomerization on the external surfaces. Although commercial ZSM-5 is more hydrophilic than the others, its strong acidity and low crystallinity result in high selectivity for 3-*t*-BEB. The optimum temperature was 300 °C, based on high conversion, and ZSM-5(25) performed better than the others.

The synthesized zeolite ZSM-5(25) showed lower conversion than the commercial ZSM-5, although both have the same Si/Al ratio. This is because the strong acid sites of the commercial zeolite are of higher strength than those of the synthesized zeolite.

3.2.2. Effects of WHSV

Since the isomerization of 4-*t*-BEB occurs on the few Brönsted acid sites present on the external surface, it could be avoided, or at least minimized, by increasing the WHSV. The results of the effects of WHSV on ethylbenzene conversion and product selectivity are presented in Table 5. The conversion decreased with increasing WHSV. As expected, the isomerization activity decreased with increasing WHSV, thus confirming our deductions. The optimum WHSV was 1.65 h^{-1}. The selectivity for 4-*t*-BEB at 6.61 h^{-1} was higher than those at the other WHSVs, but the conversion was low, so it was not the optimum value.

3.2.3. Effects of feed ratio

The feed ratio was altered to study its influence on ethylbenzene conversion and product selectivity; the results are presented in Table 6. The conversion decreased with increasing *t*-butyl alcohol content in the feed. The ZSM-5 channels could be filled with large numbers of *t*-butyl cations, and these could offer high steric hindrance to diffusion of *tert*-butylated ethylbenzene. A high alcohol content in the feed, particularly above a feed ratio of 1:1, might therefore not be

Table 5
Effects of WHSV on ethylbenzene conversion and product selectivity over ZSM-5(25).

Feed rate (ml/h)	WHSV (h^{-1})	Ethylbenzene conversion (%)	Selectivity (%)	
			3-*t*-BEB	4-*t*-BEB
1	1.65	49.3	7.6	92.4
2	3.31	43.5	5.7	94.3
3	4.96	40.2	2.5	97.5
4	6.61	30.9	1.5	98.5

Reaction conditions: temperature 300 °C, feed ratio 1:1.

Table 6
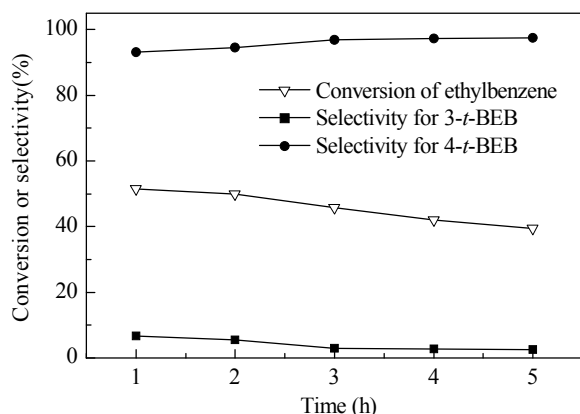Effects of feed ratio on ethylbenzene conversion and product selectivity over ZSM-5(25).

Feed ratio	WHSV (h^{-1})	Ethylbenzene conversion (%)	Selectivity (%)	
			3-*t*-BEB	4-*t*-BEB
1:1	1.65	49.3	7.6	92.4
1:2	1.62	42.7	5.5	94.5
1:3	1.61	36.2	3.9	96.1
2:1	1.68	51.5	6.8	93.2
3:1	1.69	48.8	9.2	90.8

Reaction conditions: temperature 300 °C, feed rate 1 ml/h.

conducive to high conversion. However, when the ratio was changed to 2:1, the conversion increased as there may not be many free *t*-butyl cations along the channels to offer hindrance to diffusion of 4-*t*-BEB. In other words, close adsorption of *t*-butyl cations prevents a high rate of diffusion of 4-*t*-BEB. Hence, optimizing the ethylbenzene content in the feed may be better than other alternatives for enhancing conversion; 2:1 was chosen as the optimum feed ratio. Although a large crystal size is generally good for high *para* selectivity, as discussed in the introduction, the present reaction does not depend on the shape-selective features of zeolites. As the *ortho* product is avoided as a result of steric hindrance, and the *meta* product is kinetically unfavorable, the reaction gives the *para* product preferentially. Even if the *meta* product is formed in the channel intersections, it cannot diffuse out of the pores. The *meta* product can therefore only be formed by isomerization of the *para* product on the external surface. If the external surface carries few weak acid sites, these sites can be blocked by post-modification for complete suppression of isomerization. Since ZSM-5 synthesized in a fluoride medium was highly crystalline, its isomerization activity was minimum. In addition, disproportionation was also greatly suppressed.

3.2.4. Effects of time-on-stream

The effects of time-on-stream on ethylbenzene conversion and product selectivity were studied at 300 °C with a feed ratio of 2:1; the results are shown in Fig. 10. The conversion decreased with increasing time-on-stream, but the decrease was not rapid. This was because of the medium pore size, which

does not provide mush space for coke formation inside the pores. The selectivity for 3-*t*-BEB decreased slightly with increasing time-on-stream as a result of blocking of the external surface acid sites by coke. As coke formation is very much favored on such external acid sites, these sites were gradually deactivated and isomerization also gradually decreased. The decrease in the selectivity for 3-*t*-BEB and the increase in the selectivity for 4-*t*-BEB confirmed that the latter is the precursor of the former. In addition, the deactivation of external acid sites may be more rapid than deactivation of sites lying inside the channels, as the medium pore size may not encourage coke formation, which requires a lot of space [15], as stated above. 2-*t*-BEB was not obtained during the entire period of time-on-stream. The time-on-stream study illustrates that if the few external acid sites are completely blocked by coke formation, the catalyst can give 100% selectivity for 4-*t*-BEB.

4. Conclusions

ZSM-5 synthesized in a fluoride medium is better than other zeolites for *para*-selective alkylation of aromatics or alkyl aromatics, as *trans* alkylation, disproportionation, and isomerization are suppressed. The fluoride medium provides large ZSM-5 crystals of high crystallinity, significantly improving the *para* selectivity of the catalyst. In ZSM-5, coke formation is also suppressed, because of its medium pore size. The number of external acid sites is minimized because of the high crystallinity. Even if there are few external acid sites, their activity for isomerization is rapidly lost as a result of coke deposition. By blocking such acid sites by simple post-modification, it is possible to ensure 100% *para* selectivity. A fluoride medium is therefore better than an alkaline medium for the commercial production of defect-free highly crystalline *para*-selective ZSM-5 catalysts.

References

[1] Ichioka R, Yamakawa S, Okino H, Kato H, Iwayama K, Konta H, Kitamura A. US Patent 6 040 490. 2000

[2] Zuo X, Niu F, Snavely K, Subramaniam B, Busch D H. *Green Chem*, 2010, 12: 260

[3] Chavan S A, Srinivas D, Ratnasamy P. *J Catal*, 2001, 204: 409

[4] Chu C C. US Patent 4 496 662. 1985

[5] Burress G T. US Patent 4 565 899. 1986

[6] Kaeding W W, Yannich P J, Klosek J M, Young L B. EP Patent 0 217 492. 1987

[7] Drobny J G. Handbook of Thermoplastic Elastomers. 1st Ed. New York: William Andrew Inc, 2007. 175

[8] Danilina N, Payrer E L, van Bokhoven J A. *Chem Commun*, 2010, 46: 1509

[9] Wise J J. US Patent 3 251 897. 1966

[10] Haag W O, Lago R M, Weisz P B. *Faraday Discuss Chem Soc*, 1981, 72: 317

[11] Olson D H, Haag W O. *ACS Symp Ser*, 1984, 248: 275

[12] Halgeri A B. *Bull Catal Soc India*, 2003, 2: 184

[13] Kim J H, Namba S, Yashima T. *Zeolites*, 1991, 11: 59

[14] Kim J H, Namba S, Yashima T. *Appl Catal A*, 1993, 100: 27

[15] Chen N Y, Garwood W E, Dwyer F G. Shape Selective Catalysis in Industrial Applications. 1st Ed. New York: Dekker, 1989. 26

Fig. 10. Effects of time-on-stream on ethylbenzene conversion and product selectivity over ZSM-5(25).

[16] Guth J L, Kessler H, Higel J M, Lamblin J M, Patarin J, Seive A, Chezeau J M, Wey R. *ACS Symp Ser*, 1989, 398: 176

[17] Axon S A, Klinowski J. *Appl Catal A*, 1994, 111: 29

[18] Kessler H, Patarin J, Schott-Darie C. *Stud Surf Sci Catal*, 1994, 85: 75

[19] Nayak V S, Riekert L. *Appl Catal*, 1986, 23: 403

[20] Paparatto G, Moretti E, Leofanti G, Gatti F. *J Catal*, 1987, 105: 227

[21] Arsenova-Härtel N, Bludau H, Schumacher R, Haag W O, Karge H G, Brunner E, Wild U. *J Catal*, 2000, 191: 326

[22] Umamaheswari V, Palanichamy M, Arabindoo B, Murugesan V. *Proc Indian Acad Sci Chem Sci*, 2002, 114: 203

[23] Bidart A M F, Borges A P S, Chagas H C, Nogueira L, Lachter E R, Mota C J A. *J Braz Chem Soc*, 2006, 17: 758

[24] Louis B, Kiwi-Minsker L. *Microporous Mesoporous Mater*, 2004, 74: 171

[25] Gougeon R D, Brouwer E B, Bodart P R, Delmotte L, Marichal C, Chezeau J M, Harris R K. *J Phys Chem B*, 2001, 105: 12249

[26] Treacy M M J, Higgins J B. Collection of Simulated XRD Powder Patterns for Zeolites. 4th Ed (Rev). Amsterdam: Elsevier, 2001. 239

[27] Woolery G L, Kuehl G H, Timken H C, Chester A W, Vartuli J C. *Zeolites*, 1997, 19: 288

[28] Sano T, Wakabayashi S, Oumi Y, Uozumi T. *Microporous Mesoporous Mater*, 2001, 46: 67

[29] Jeffery G H, Bassett J, Mendham J, Denney R C. Vogel's Textbook of Quantitative Chemical Analysis. 5th Ed. UK: Longman, 1989. 833

[30] Arichi J, Louis B. *Cryst Growth Des*, 2008, 8: 3999

[31] Kim J H, Park M J, Kim S J, Joo O S, Jung K D. *Appl Catal A*, 2004, 264: 37

[32] Vishwanathan V, Jun K W, Kim J W, Roh H S. *Appl Catal A*, 2004, 276: 251

[33] Kim S D, Baek S C, Lee Y J, Jun K W, Kim M J, Yoo I S. *Appl Catal A*, 2006, 309: 139

[34] Bortnovsky O, Sazama P, Wichterlova B. *Appl Catal A*, 2005, 287: 203

[35] Seiler M, Wang W, Hunger M. *J Phys Chem B*, 2001, 105: 8143

[36] Grieken R V, Sotelo J L, Menéndez J M, Melero J A. *Microporous Mesoporous Mater*, 2000, 39: 135

[37] Liu Z, Moreau P, Fajula F. *Appl Catal A*, 1997, 159: 305

[38] Schaefer T, Chan W K, Sebastian R, Schurko R, Hruska F E. *Can J Chem*, 1994, 72: 1972

Graphical Abstract

Chin. J. Catal., 2013, 34: 294–304   doi: 10.1016/S1872-2067(11)60482-8

Effects of crystallinity of ZSM-5 zeolite on *para*-selective *tert*-butylation of ethylbenzene

PUSHPARAJ Hemalatha, MANI Ganesh, MUTHIAHPILLAI Palanichamy, VELAYUTHAM Murugesan, PARK Yong-Ki, CHOI Won Choon, JANG Hyun Tae*
Hanseo University, South Korea; Anna University, India; Korea Research Institute of Chemical Technology, South Korea
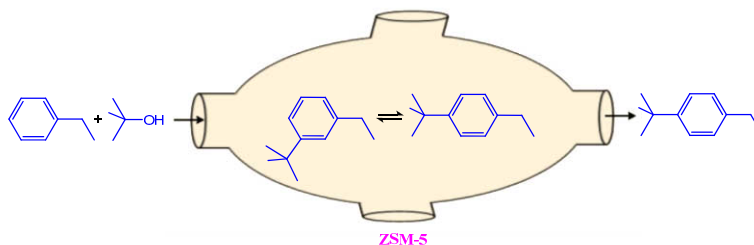
A fluoride medium offers defect-free, highly crystalline ZSM-5 crystals. High crystallinity confers high *para* selectivity (> 90%) in *tert*-butylation of ethylbenzene. A fluoride medium is better than an alkaline medium for the commercial production of *para*-selective ZSM-5 catalysts.